Published in: Topics in Catalysis 14 (2001) 111-123

Understanding Heterogenous Catalysis on an Atomic Scale: A Combined Surface Science and Reactivity Investigation for the Dehydrogenation of Ethylbenzene over Iron Oxide Catalysts

C. Kuhrs, Y. Arita, W. Weiss, W. Ranke* and R. Schlögl

Department of Inorganic Chemistry, Fritz-Haber-Institut of the MPG, Faradayweg 4-6, 14195 Berlin, Germany.

* Corresponding author: e-mail ressler@fhi-berlin.mpg.de, phone +49 30 8413 4523, fax +49 30 8413 4401

Abstract:

In order to study the dehydrogenation of ethylbenzene to styrene, epitaxial iron oxide model catalyst films with $Fe_3O_4(111)$, α-$Fe_2O_3(0001)$ and $KFe_xO_y(111)$ stoichiometry were prepared in single crystal quality on Pt(111). They were investigated using surface science techniques before and after atmospheric pressure reaction experiments in a newly designed single crystal flow reactor. As expected from low pressure measurements, $Fe_3O_4(111)$ is catalytically inactive. The catalytic activity of α-$Fe_2O_3(0001)$ starts after an activation period of about 45 minutes. After that, the surface is essentially clean but shows a high concentration of defects. On the potassium promoted films, however, the activation period is much longer, the activity then is higher and the surface gets covered completely with carbon and oxygen during reaction. This indicates a different reaction pathway on the promoted films with a carbon-oxygen species as catalytically active species.

Keywords: metal oxides; atomic scale surface chemistry; TDS; single crystal flow reactor; high pressure; pressure gap; defects; active carbon

1. Introduction

Oxide catalysts are used for many important synthesis reactions in chemical industry, but hardly anything is known about the relationships between their catalytic function, chemical compositions and crystallographic structure.
In the model catalysis approach, these questions are tackled by preparing surfaces with defined surface structure and composition, on which elementary step kinetics can be investigated in a first step under ultrahigh vacuum (UHV) conditions [1,2]. In the second step, catalytic reactions have to be performed on these model catalysts under conditions that should be as close to the technical catalytic conditions as possible. The pressure-gap between the UHV experiments and the experiments performed under real conditions is bridged if low pressure and high pressure reaction kinetics can be described by the same model. Together with post reaction surface analysis insight into the atomic scale chemistry can be obtained.
Whereas there are some examples in literature for combining high pressure catalytic reaction studies with UHV surface analytical techniques for metals [3,4], only one attempt has been made so far to apply this concept to metal oxide based catalysts [5].

The dehydrogenation of ethylbenzene to styrene is a large scale industrial reaction that is carried out at 870 K over iron oxide catalysts in the presence of steam [6]. As it is possible to prepare epitaxial iron oxide films of different stoichiometry on Pt(111) single crystals [7], ideal model catalysts for this reaction are available. Recently also an ordered potassium promoted iron oxide film was prepared [8]. This is of special interest as potassium is the main promotor for industrial catalysts and increases the conversion rate by about one order of magnitude [9].
For the combination of UHV experiments carried out on these films and catalytic conversion tests performed under atmospheric pressure, a newly designed single crystal flow reactor was build [10] and successfully operated [11].
Here we proceed in the following way: Epitaxial $Fe_3O_4(111)$, α-$Fe_2O_3(0001)$ and $KFe_xO_y(111)$ films are characterized in UHV concerning their structure and composition. Then thermal desorption spectroscopic (TDS) measurements of the reaction educt ethylbenzene (EB) and of the product styrene (St) are carried out and compared with high pressure catalytic conversion tests. Finally, in post-reaction measurements, the structures, compositions and TDS properties are checked again in UHV. Different reaction mechanisms on the different samples and the question of the existence of a pressure gap are discussed.

2. Experimental

As described in detail previously [7], well ordered epitaxial $Fe_3O_4(111)$ and α-$Fe_2O_3(0001)$ films were grown onto Pt(111) samples by repeated cycles of iron deposition and subsequent oxidation at different oxygen pressures. The potassium promoted $KFe_xO_y(111)$ films were prepared by potassium deposition onto an epitaxial $Fe_3O_4(111)$ film and subsequent annealing as described in [8]. They form a well ordered hexagonal surface structure with a (2x2) superstructure with respect to $Fe_3O_4(111)$. The oxide films and the KFe_xO_y film can easily be distinguished by their low energy electron diffraction (LEED) patterns [7]. Typical patterns are included as inserts in Fig. 1 and Fig. 2. All films were 10-30 nm thick. Thermal desorption spectroscopic (TDS) measurements were performed using a quadrupole mass spectrometer in an UHV chamber [12] which was further equipped with a LEED optics and a cylindrical mirror analyser (CMA) for Auger electron spectroscopy (AES). Ethylbenzene (EB) and styrene (St) were adsorbed onto the samples at 100 K with exposures given in Langmuir units (1 L = $1.33x10^{-6}$ mbar s), the heating rate for TDS was always 5 K/s. After each run the films were briefly heated at 870 K in 10^{-6} mbar oxygen in order to remove residual cracking products.

Ion scattering spectroscopy (ISS) measurements were performed in a second analysis chamber separated by a gate valve from the TDS chamber to which the sample could be transferred under vacuum. A commercially available Omicron system with helium as scattering gas was used. ISS measurements reveal information about the chemical composition of the topmost layer of the surface under investigation.

STM measurements were performed in a separate chamber which is described in [12].

A flow reactor designed for the investigation of heterogeneous catalytic reactions on single crystalline metal oxide model catalysts was used. It is located in a high pressure cell that is attached to the TDS analysis chamber, from which it can be completely separated by a gate valve. The high pressure cell was also used for the preparation of the α-Fe_2O_3 films from Fe_3O_4 by high pressure oxidation. After transfer of the samples into the flow reactor cell, it was vented with nitrogen. A constant He carrier gas flow of 10 and 40 ml/min passed through reservoirs with liquid EB and water held at T=30°C before mixing both. This provides an ethylbenzene partial pressure of 3.3 mbar and a water partial pressure of 33.5 mbar (EB:H_2O=1:10). This gas mixture entered the reaction volume (roughly 4 ml) through a capillary of 0.2 mm inner diameter. In the reactor the sample was heated from behind by two high power fiber-coupled diode lasers with a combined optical output power of 100 W. From the product gas mixture, units of 250 µl were injected every three minutes from a sample loop into the column of a gas chromatograph with a mass spectrometer (GC/MS) with high detection sensitivity. All gas lines were heated resistively to prevent condensation of educt and product molecules. For more details see ref. [10].

3. Results

3.1 Pre reaction UHV studies: Adsorption of ethylbenzene and styrene

Fig. 1 shows TDS traces after exposing $Fe_3O_4(111)$, α-$Fe_2O_3(0001)$ and $KFe_xO_y(111)$ to different amounts of ethylbenzene. At low exposure of EB on Fe_3O_4 (Fig. 1a), a chemisorbed species labelled γ appears at around 420 K. With increasing exposure, it shifts very strongly down to 250 K. It saturates at around 1 L. With increasing exposure, additional physisorbed (β) and condensed (α) species appear. At low exposures of EB on Fe_2O_3 (Fig. 1b), a small peak γ_2 appears at about 370 K, which is saturated even at the lowest exposure of 0.11 L. A sharp peak γ_1 follows starting to desorb at 275 K and shifting with coverage to 260 K. It saturates at about 1 L. Similar to the Fe_3O_4 film, physisorbed and condensed species follow upon higher exposures. At low exposure of EB on the potassium promoted KFe_xO_y multilayer film (Fig. 1c), a peak γ appears. It starts to desorb at about 265 K, shifts to 260 K and saturates also at about 1 L. At higher exposures, again physisorbed and condensed states appear.

Fig. 2 shows corresponding TDS traces for styrene. At low exposures of St on Fe_3O_4 (Fig. 2a), a chemisorbed species γ_2 appears at around 480 K, clearly at a higher temperature than the γ species of EB in Fig. 1a. This indicates a stronger binding of the styrene molecule to the substrate. With increasing exposure, the signal shifts to 260 K (γ_1) and saturates at about 1-1.3 L comparable to the observations made for the γ species of EB. Wheras for ethylbenzene a very broad signal is observed, two different adsorption states γ_2 and γ_1 can be distuingished for styrene. TD spectra of St adsorbed onto the Fe_2O_3 film are shown in Fig. 2b. The γ_2 peak looks exactly the same as that for EB having the same desorption temperature, too. Also the styrene γ_1 peak is very similar to the ethylbenzene γ_1 peak. It saturates at about 1.3 L but starts to desorb at a slightly higher temperature (300 K) and shifts with exposure down to 260 K. For the $KFe_xO_y(111)$ film (Fig. 2c), there is no difference in the γ peak position of EB and St. Physisorbed and condensed styrene is observed on all films upon higher exposures.

On all investigated films, mobile extrinsic precursor species which can migrate over occupied sites and eventually adsorb at vacant sites can be assumed [13]. Especially for the γ species on the Fe_3O_4 film, a sequential filling from strongly to more weakly bound adsorption states can be observed which shows that a molecule impinging onto the surface can move to find the most strongly bound still unoccupied state.

In order to compare the desorption properties of EB and St, TDS traces of the low coverage chemisorbed species are reproduced in Fig. 3. For both EB and St, the relative bond strength of chemisorption decreases from Fe_3O_4 over Fe_2O_3 to the potassium promoted Fe_3O_4 film. The difference of the bond strength between styrene and ethylbenzene also decreases in this direction. On Fe_3O_4, styrene is much more strongly bound than ethylbenzene, only slightly more strongly on Fe_2O_3, and on the KFe_xO_y film there is no more difference between the bond strength of styrene and ethylbenzene.

An exposure of 1 L of EB or St at a gas temperature of 300 K corresponds to $1.96x10^{14}$ molecules cm^{-2} impinging onto the surface. The Van-der-Waals area of EB and styrene molecules lying flat on the surface is approximately 50 $Å^2$, so that 1 ML corresponds to N=$2x10^{14}$ molecules cm^{-2}, assuming a densely packed layer. Since condensation occurs at 150 K for these molecules, a sticking probability of 1 can be assumed for the sample temperature of 100 K during adsorption, so that the observed saturation exposure of the chemisorbed γ species of 1 L corresponds to about 1 ML which indicates adsorption on regular surface areas.

The amount of chemisorbed species decreases as the surface defect concentration increases (as deduced qualitatively from the signal background ratio in LEED), and no additional adsorption states with higher binding energies appear on defective films. Thus, no specific chemisorption at defects exists, and adsorption sites located near defects must

have the same adsorption energies as adsorption sites located far away from defects.

The different chemisorption strenght for EB and St on $Fe_3O_4(111)$, $Fe_2O_3(0001)$ and $KFe_xO_y(111)$ can be understood within the Lewis acid-base picture. EB and St are highly polarizable soft Lewis bases interacting strongly with the $Fe_3O_4(111)$ surface exposing soft acidic Fe^{2+} sites [14]. $Fe_2O_3(0001)$ exposes hard acidic Fe^{3+} sites and consequently, the interaction becomes weaker and on $KFe_xO_y(111)$, the interaction is weakest since K^+ is a hard acidic site with a very low electron affinity [15]. In general, the chemisorption strength of EB and St decreases with increasing Lewis hardness of the metal oxide surface. Styrene interacts more strongly than ethylbenzene on Fe_3O_4 and Fe_2O_3 because of the additional unsaturated C-C bond contributing to the polarizable π-electron orbitals. On $KFe_xO_y(111)$, the interaction is so weak that no difference between EB and St can be observed anymore. From the TDS data the desorption energies E_{des} and frequency factors ν_{des} of the chemisorbed species were determined by a threshold analysis [16]. They are listed in table 1.

3.2 Extrapolation across the pressure-gap

Using the Langmuir isotherm the relative coverage Θ_r (number of occupied divided by the number of available adsorption sites) under adsorption-desorption equilibrium conditions [17] can be estimated:

$$\Theta_r = bp/(1+b\,p)$$

with p being the gas pressure and b given by

$$b = \{s_0/(\nu_{des}\, N\, (2\pi mkT)^{0.5})\}\, \exp\{-(\Delta E_{ad}-\Delta E_{des})/kT\}.$$

Here, s_0 is the initial sticking coefficient, N the adsorption site density which is $2x10^{14}$ cm^{-2} for EB and St[8], m the mass of the adsorbing molecule, k the Boltzmann constant, T the temperature, and ΔE_{ad}, ΔE_{des} the activation energies for adsorption and desorption, respectively. For competitive coadsorption of two different molecules A and B, we obtain

$$\Theta_{r,A} = b_A\, p_A/(1+b_A\, p_A+b_B\, p_B), \quad \Theta_{r,B} = b_B\, p_B/(1+b_A\, p_A+b_B\, p_B), \text{ and } \Theta_r = \Theta_{r,A} + \Theta_{r,B}.$$

Here, p_A and p_B are the partial pressures (in units of Pascal) of gases A and B, respectively.

As discussed in [8], the surface coverages of EB and St under technical styrene synthesis reaction conditions (T = 873 K, p_{EB} or p_{St}=200 mbar) can be estimated by this approach using the desorption energies and frequency factors from table 1. We assume initial sticking coefficients s_0=1 for both molecules and non-activated adsorption ($\Delta E_{ad} \approx 0$). The occupation of physisorbed and condensed states is always low under reaction conditions and is neglected.

On $Fe_3O_4(111)$, the Langmuir extrapolation yields $\Theta_r = \Theta_{r,EB} + \Theta_{r,ST} = 100\%$ and $\Theta_{EB}/\Theta_{ST} \approx 0.004$; on α-$Fe_2O_3(0001)$ it yields $\Theta_r = 35\%$ and $\Theta_{EB}/\Theta_{ST} \approx 1.3$, and on $KFe_xO_y(111)$ $\Theta_r = 18\%$ and $\Theta_{EB}/\Theta_{ST} \approx 5$ are obtained. Thus on $Fe_3O_4(111)$ all chemisorption sites are occupied ($2x10^{14}$ molecules per cm^2), on $Fe_2O_3(0001)$ 35%, and on $KFe_xO_y(111)$ 18%. For the catalytic dehydrogenation reaction of EB to St the relative occuppation of these sites by EB and St, Θ_{EB}/Θ_{ST}, is important. On Fe_3O_4 all chemisorption sites are blocked by the product molecule styrene, on Fe_2O_3 43% of these sites are occupied by styrene, and on KFe_xO_y only 17% are occupied by styrene. This would agree with an increasing catalytic activity when going from Fe_3O_4 over Fe_2O_3 to KFe_xO_y.

3.3 Reactor experiments

Reactor experiments under atmospheric pressure were carried out in the newly designed single crystal flow reactor that is described in detail in [10]. The reaction temperature was 870 K. Assuming saturation of the helium carrier gas with ethylbenzene and water, $6.7x10^{-6}$ mol/min of EB and $6.7x10^{-5}$ mol/min of water entered the reactor. With a reactor volume of about 4 ml and a total gas flow of 50 ml/min a residence time of about 5 s can be estimated.

A small amount (250 µl) of the product gas is injected every three minutes into the column of a gas chromatograph. The gas chromatogram shows therefore a peak or a set of peaks every three minutes which can be analysed by a mass spectrometer.

The gas chromatogram with the $Fe_3O_4(111)$ in the reactor is shown in Fig. 4. Only one peak is observed every three minutes. The mass spectrum (Fig. 4, lower part) for one of these peaks indicates that only ethylbenzene with m/z=106 and its main cracking product with m/z=91 is present. Thus no conversion to styrene occurs on Fe_3O_4.

For Fe_2O_3 and KFe_xO_y, the situation is different. After a certain activation period t_{act}, a small second peak right to the main ethylbenzene peak appears in the gas chromatogram. A part of the gas chromatogram where this second peak (marked by arrows) appears for the KFe_xO_y film is shown in Fig. 5 together with the mass spectrum of one of them. The main contribution is m/z=104, corresponding to styrene. The contributions at m/z=106 and 91 are due to the tail of the ethylbenzene main peak in the GC curves. Fig. 6 shows the temporal evolution of the activity of both films. Wheras conversion to styrene starts on the Fe_2O_3 film after an activation period of about 45 minutes, about 2 hours are necessary for KFe_xO_y. The activation period t_{act} varied in certain limits between different experiments but it was always 2-3 times larger on the KFe_xO_y film than on Fe_2O_3. On both films, the steady state is reached within a short time after activation has started. On the KFe_xO_y film, a conversion rate of about 3.5 % with respect to the amount of ethylbenzene introduced is observed and on the Fe_2O_3 film it reaches 1.5 %.

In comparison to technical catalysts, the maximum conversion per surface area and time is about one order of magnitude higher here. This is probably due to the fact that the flow of educt molecules per catalyst surface area is 10^4 times higher compared to technical reactors which is necessary to obtain a gas flow that is high enough to be handled with gas supply devices. The higher amount of educt in this experiment shifts the equilibrium to the product side and leads to higher absolute but to lower relative conversion in comparison to technical catalysis conditions.

3.4 Post reaction analysis

Fig. 7 shows Auger spectra of the α-Fe_2O_3 and the KFe_xO_y model catalyst films before and after reactor experiments. After the reaction experiments, a small carbon signal appears on $Fe_2O_3(0001)$ (Fig. 7a). The oxygen to iron ratio has slightly increased.

Before the reactor experiment only potassium, oxygen and iron can be detected on the KFe_xO_y film with peak height ratios characteristic for the film showing the (2x2) LEED pattern (Fig. 7b). After reaction, a big carbon signal has appeared. The iron signal is diffuse and strongly reduced. Also the potassium signal is reduced but because of its overlap with the carbon signal, no clear separation can be made.

Here, surface sensitive ISS measurements are helpful. Fig. 8 shows that before reaction only oxygen and potassium can be clearly identified in the topmost layer, possibly together with traces of iron (Fig. 8a). The active film after reaction shows only carbon and oxygen suggesting that an active

carbon-oxygen species exists on the surface (Fig. 8b). TDS measurements (Fig. 9) of ethylbenzene on this carbon-oxygen covered films yield only a physisorbed β and a condensed α species. This shows clearly that the original KFe_xO_y surface with its more strongly bound γ state is completely replaced and cannot as minority domains be responsible for the catalytic activity. On the Fe_2O_3 film, the chemisorbed species can still be detected after a reaction experiment but with less intensity (not shown here).

In Fig. 10, LEED images of a Fe_2O_3 film before and after the reaction experiment are compared. After the reaction experiment, the LEED spots have broadened and the background increased indicating a considerable increase of defects. On the other hand, the characteristic Fe_2O_3 pattern can still be identified showing that the stoichiometry of the film does not change and is important for catalytic activity. For KFe_xO_y, the LEED image was always completely diffuse after reaction.

Also STM measurements show that the surface roughness has increased considerably after reaction. This is demonstrated in the topographic survey scans and line scans for Fe_2O_3 and KFe_xO_y in Fig. 11.

Post-reaction Auger and LEED measurements on the inactive Fe_3O_4 film indicated some carbon deposits and also an increase of surface roughness.

4. Discussion

For the dehydrogenation of ethylbenzene to styrene, Fe_3O_4 proved to be inactive. Fe_2O_3 becomes active after an induction period of about 45 minutes. Post reaction analysis showed that the surface still was Fe_2O_3 with only a small contamination by carbon deposits. However, the defect concentration had increased considerably. Obviously, the activation period is necessary for the creation of defects. Although defects do not adsorb the educt or product molecules strongly – TDS shows no new adsorption states – they are necessary for the conversion reaction. The activity for conversion is not increasing continuously but starts suddenly and reaches its maximum within only a few minutes. The formation of an active surface phase, initiated by a nucleation process, may be suspected. The activation period for KFe_xO_y is considerably longer. Also here, activity develops suddenly within a few minutes. Post reaction analysis shows that the surface is completely covered by a disordered layer consisting of carbon and oxygen.

The results presented here and additional information from earlier surface analytical experiments [18] on technical iron oxide catalysts will be used to identify possible modes of action of the iron oxide in the EB dehydrogenation.

The TDS data revealed that Fe_3O_4 is no suitable catalyst because of the strong chemisorption of the initially formed product styrene. This is due to blocking of the regular surface with styrene which inhibits the adsorption of new educt molecules and thus prevents the active sites to come into action. This perception is in good agreement with surface analytical findings from technical catalysts that the abundance of divalent iron at the surface is not inhibiting the catalytic activity.

Pure Fe_2O_3 is a moderately active catalyst after in-situ formation of active sites. The AES results indicate a slight increase of the oxygen to iron ratio and the LEED pattern contains an increased diffuse contribution after reaction. This suggests the co-existence of strongly disordered patches of ferric oxide with residual defect-poor and hence non-reactive regions of the surface. Despite the co-existence of iron- and oxygen termination it is assumed that oxygen atoms in a different height relative to the iron atoms have to act as dehydrogenation centers. This becomes clear when the shape of the EB molecule is taken into account. The ethyl rest is bent by about 100° relative to the plane of the aromatic carbon atoms which collectively interact with the iron atoms on the surface. The location of the chemical transformation (the ethyl group) is either above or below this plane which requires oxygen atoms above (on upwards steps) or below (at holes or downwards steps) of the terrace plane of the iron oxide. The situation is represented in Fig. 12.

This scheme reveals that the active site is a rather complex ensemble of atoms involving atoms from several atomic layers of the catalyst. The maximisation of the abundance of such ensembles can be envisaged as a difficult in-situ rearrangement of the catalysts surface microstructure and may well account for the induction time observed in the high pressure reaction experiment.

At the oxygen sites of the defect, the elementary step of dehydrogenation of the ethyl to an ethylene group takes place. Concomitant to this hydrogen abstraction there is also the transition of two electrons from the ethyl carbon atoms to the catalyst thus reducing the iron atoms adjacent to the receiving oxygen atoms. We assume that the iron atom which is required for the fixation of the EB molecule is not reduced in its valence as then the interaction with the aromatic ring would be strengthened resulting in a site blocking. Even though we do not know how the electron transfer occurs, a reduction of the Fe^{3+} ions near the oxygen anions receiving the hydrogen seems to be reasonable.

After desorption of the product molecule a reduced catalyst with two OH groups and two Fe^{2+} sites remains. This represents the deactivated state and reactions are required in order to restore the active site. The homolytic cleavage of the OH groups leading to the by-product hydrogen would be a difficult reaction as the O-H bond strength in the deactivated state is expected to be strong. Otherwise the cleavage of two only weakly activated C-H bonds in the ethyl group would hardly occur. The deprotonation of the OH groups may be the rate-limiting step in the overall process as the surface analytical investigation showed that clear inverse correlation exists between the abundance of surface O-H groups and the EB conversion.

Two different scenarios can be envisaged for the regeneration of the active site. One scenario assumes that the O-H groups are cleaved homolytically using the two electrons stored at the two OH adjacent iron atoms thus producing one molecule of dihydrogen. Such reactions are also discussed in other areas of C-H activation catalysis where the formation of a cyclic metal hydride state is envisaged which reacts with the neighbouring proton from the second O-H group.

In conventional chemistry ferrous oxyhydroxide would not react to ferric oxide and hydrogen but would disproportionate to ferric oxide, iron metal and molecular water. In a consecutive reaction the iron metal could react with a water molecule to form ferric oxide and dihydrogen. In analogy to this it may well be that the deactivated site looses one molecule of water and retains one iron site reduced below the Fe^{2+} state. The initial geometry could be restored by dissociation of a water molecule from the feed. The advantage of this scenario would be that this dissociation could be temporally and locally decoupled. In this sense the overall reaction would be an oxydehydrogenation and the co-feed water would be an essential reactant serving as a mild oxidant for highly reduced iron sites. One of the elementary steps of the oxydehydrogenation scenario could further account for the formal activation energy which was reported to be between 100 and 150 kJ/mole which is considerably higher than any desorption energy determined here (see table 1).

The significantly enhanced productivity as well as the post-reaction analytical data imply that the potassium-modified Fe_3O_4 may react according to a different scenario. The absence of any iron and potassium at the activated surface would imply that a carbon-oxygen structure could be actively involved in the process. The earlier surface analytical data did not support a systematic correlation between carbon

abundance and EB conversion. As the depth of information of XPS is much larger (electron mean free path ca. 2 nm) than for the ISS method (topmost atomic layer only) and no surface free of carbon was found in the post-reaction XPS analysis, the active participation of oxygenated graphitic carbon in the EB conversion reaction cannot be ruled out.

The high coverage of the iron oxide with carbon in the presence of potassium follows the notion that a Broensted-basic surface initiates the polymerisation of styrene to polystyrene which is consecutively dehydrogenated to graphite-like structures. The shape of the carbon AES signal in Figure 7 as well as earlier observations clearly indicate the aromatic character of the deposit. This deposit is obviously involved in the reaction which would be in line with the extensive activation time required for the potassium-promoted iron oxide to become active. Cases of "invisible" or "harmless" carbon deposits are well documented from the surface analysis of Pt-hydrogenation catalysts [19]. Such carbon forms an optically dense but for molecules easy to penetrate overlayer over the still active catalyst. Ethylbenzene TDS measurements on the activated KFe_xO_y catalyst, however, only show physisorbed and condensed species clearly indicating that the molecules do not "feel" the original substrate any more. It is known that functionalised carbon is a suitable catalyst for oxydehydrogenation of EB with oxygen [20]. At 600 K this reaction reaches about 45 % conversion with about 80 % selectivity to styrene. The carbon catalyst is also covered with "coke" in amounts which could be easily weighted. This coke did not either inhibit the reaction and was speculated to be active in the reaction. Also on other metal oxide catalysts it was observed that coke formation did not inhibit the reaction and might be active in the reaction [21].

In the present reaction there is formally no oxidant like molecular oxygen fed with the EB. This and the stoichiometric evolution of hydrogen as second reactant did always lead to the conclusion that the reaction scenario should be a dehydrogenation with the hydrogen stemming from the EB ethyl groups. This can, unfortunately, not be verified by isotope marker experiments as the high basicity of the catalysts initiates immediate scrambling between water and labelled EB even under conditions totally non-reactive for styrene formation.

At present the view that on highly carbon-covered catalysts the EB conversion operates with an in-situ formed carbon catalyst [22] has to remain a speculation. In this scenario the iron oxide would be required to split water into hydrogen and oxygen. This could follow a defect mechanism in the same way as discussed with the mode of action of pure Fe_2O_3. The oxygen formed from water would have to react with carbon to form a labile carbon oxygen complex which are also well known to exist [23].

It is also well-known that potassium strongly catalyses the formation of carbon-oxygen functionalities which operates then even with less oxidising molecules than water such as $CO_{2[24]}$. Also the formation of very strongly basic carbon oxygen functions such as quinone structures [25] is feasible which would act as a secondary catalyst for the dehydrogenation of EB.

These considerations imply that the function of the potassium promoted iron oxide film in EB conversion may well be fundamentally different from that of the binary oxide model system. The presence of the potassium ions at the surface (see ISS), the complex and mostly rough surface morphology with its many defects [26] and the still unknown overall electronic structure of this species of model films may be responsible for this behaviour. Conventional surface characterisation on the used model catalysts is difficult as illustrated with Figures 10 and 11 due to the massive abundance of disordered species in the oxide and from the carbon deposits.

5. Conclusions

The successful operation of a single pass high pressure reactor for model films of iron oxides in the EB dehydrogenation reaction has brought new insights into the mode of action of the catalyst. The excellent catalytic performance even under imperfectly controlled kinetic conditions (no defined residence time) suggests that the reactor design of a multitubular plug flow arrangement with macroscopic catalysts extrudates as often used today may not be the optimum reaction environment for the process. The high specific activity we observed here is attributed to the better control of transport properties and of the solid state reactions leading to the essential surface modification for the catalytic function. One would conclude that thin films or small particles of the active component iron oxide in a defective form on a heat-conducting support which does not catalyse the polymerisation of the product could increase the technical systems performance even in existing reactors. The recently suggested application of membrane reactors would offer many possibilities to apply a catalyst in similar forms as the model system used here [27].

The exact reproduction of the relative activity sequence for polycrystalline materials and the model systems lends strong support to the conjecture that the strong differences in chemisorption behaviour of educt and product on these model films also plays a decisive role in controlling the microkinetics of the process. Several important aspects of the reaction remain still highly speculative at this point. Further experiments on this series of model systems will, however, allow us to clarify several points. It may be that during this classification it will occur that the surface interaction between EB and potassium promoted catalysts is not the main relevant reaction channel but may only be needed to produce a carbon-based active mass which solely forms under the working conditions of the reaction. The non-existence of a chemisorbed EB-species on a highly carbon loaded catalyst film is a first strong hint for such a mechanism. This possibility shows the limitation of model investigations carried out at low pressure and low conversion which not only may favour the focusing of investigations onto non-relevant reaction channels but may neglect reactions with massive alterations of the catalyst chemistry.

Acknowledgements

We thank G. Ketteler and Sh. K. Shaikhutdinov for performing the STM measurements.

References

[1] H.-J. Freund; Angewandte Chemie **109/5** (1997) 444.
[2] V.E. Henrich and P.A. Cox, The Surface Science of Metal Oxides, Cambridge Univ. Press, Cambridge, 1994.
[3] B.A. Sexton and G.A. Somorjai; J. Catal. **47** (1977) 167.
[4] D.J. Dwyer and G.A. Somorjai, J. Catal. **52** (1978) 291.
[5] M. Bender, A. Knocks, S. Hövel and H.-J. Freund; in Proceedings of the first International Conference on Microreaction Technology, Springer, Ed.: W. Ehrfeld (1997) 55.
[6] E.H. Lee; Calal. Rev. **8** (1973) 285.
[7] W. Weiss; Surf. Sci. **377** (1997) 943.

[8] Sh. K. Shaikhutdinov, Y. Joseph, C. Kuhrs, W. Ranke and W. Weiss; Faraday Discussions **114** (1999) 363.
[9] T. Hirano; Appl. Catal. **26** (1986) 65.
[10] C. Kuhrs, M. Swoboda, W. Weiss; Topics in Catalysis, in press.
[11] C. Kuhrs and W. Weiss; Stud. Surf. Sci. Catal., in press.
[12] W. Weiss, M. Ritter, D. Zscherpel, M. Swoboda and R. Schlögl; J. Vac. Sci. & Technol. **A 16** (1998) 21.
[13] D. Zscherpel, W. Weiss and R. Schlögl; Surf. Sci. **382** (1997) 326.
[14] W. Weiss and R. Schlögl; submitted to Topics in Catalysis.
[15] J. E. Huheey; W. de Gruyter, Berlin (1987) 339.
[16] E. Habenschaden, J. Küppers; Surface Science **138** (1984) L147.
[17] K. Christmann; Surface Physical Chemistry, Steinkopff, Darmstadt 1991.
[18] M. Muhler, R. Schlögl and G. Ertl; J. of Catal. **138** (1992) 413.
[19] Z. Paal, R. Schlögl, G. Ertl; Faraday Trans. **88** (1992) 1179.
[20] R. S. Drago, K. Jurczyk; Appl. Catal. A **112** (1994) 117.
[21] G. Emig and H. Hofmann; J. Catal. **84** (1983) 15.
[22] H. P. Boehm, G. Mair, T. Stoehr, A. R. de Rincon, B. Tereczki; Fuel **63** (1984) 1061.
[23] J. A. Moulijn, F. Kapteijn; Carbon **33** (1995) 1155.
[24] M. B. Cerfontain, R. Meijer, F. Kapteijn, J. A. Moulijn; J. Catal. **107** (1987) 173.
[25] M. Voll, H. P. Boehm; Carbon **9** (1971) 481.
[26] Sh. K. Shaikhutdinov, W. Weiss, R. Schlögl; Appl. Surf. Sci, in press
[27] R. Dittmeyer, V. Hollein, P. Quicker, G. Emig, G. Hausinger, F. Schmidt; Chem. Ing. Sci. **54** (1999) 1431.

Table 1: Desorption energies E_{des} and frequency prefactors ν_{des} for the chemisorbed γ species of EB and St on $Fe_3O_4(111)$, α-$Fe_2O_3(0001)$ and $KFe_xO_y(111)$ at low coverages, as determined from the TDS measurements. In the lower part, ratios for the conversion of ethylbenzene to styrene in percent in the high pressure reaction measurement are shown.

$Fe_3O_4(111)$			**a-$Fe_2O_3(0001)$**			**$KFe_xO_y(111)$**		
	ethyl-benzene	styrene (γ_2)		ethyl-benzene	styrene		ethyl-benzene	styrene
γ: E_{des}	86 kJ/mol	118 kJ/mol	γ_1: E_{des}	64 kJ/mol	73 kJ/mol	γ: E_{des}	65 kJ/mol	65 kJ/mol
γ: ν_{des}	$1x10^{12}$ s^{-1}	$3x10^{11}$ s^{-1}	γ_1: ν_{des}	$1x10^{12}$ s^{-1}	$5x10^{12}$ s^{-1}	γ: ν_{des}	$2x10^{12}$ s^{-1}	$1x10^{13}$ s^{-1}
0 %			1.5 %			3.5 %		

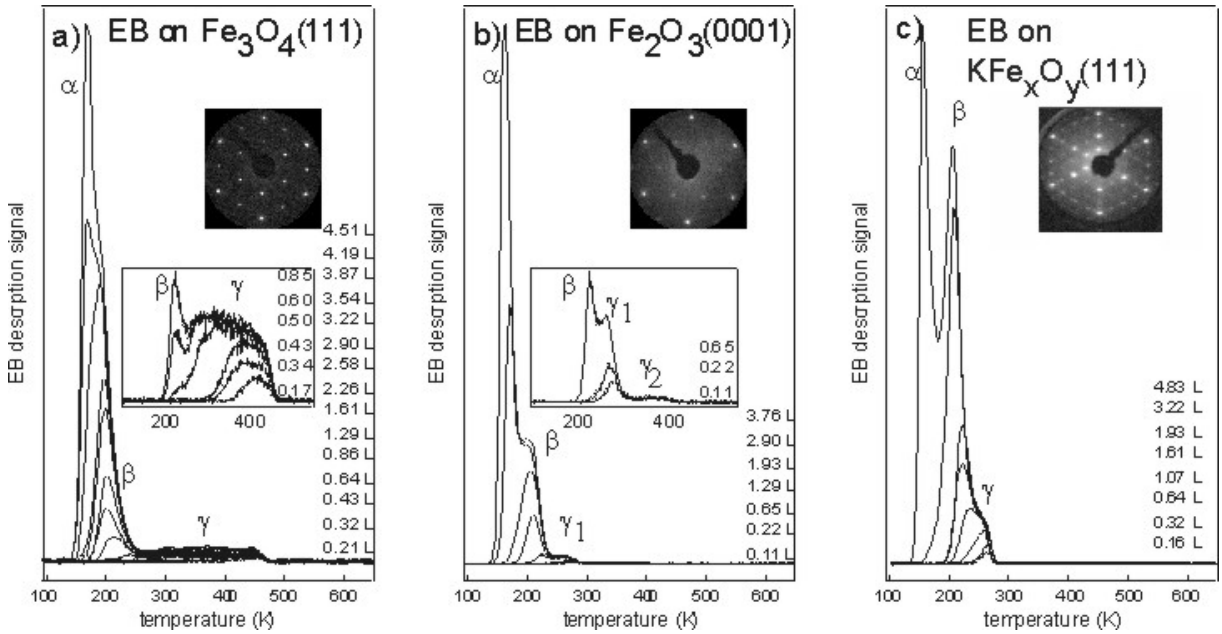

Fig. 1: TD spectra of ethylbenzene (EB) absorbed at T=100 K onto Fe_3O_4(111), α-Fe_2O_3(0001) and KFe_xO_y(111). The exposures are given in Langmuir units. The inserts show magnified TD traces for low exposures. Additionally, LEED patterns of the corresponding clean films taken at E=60 eV are shown.

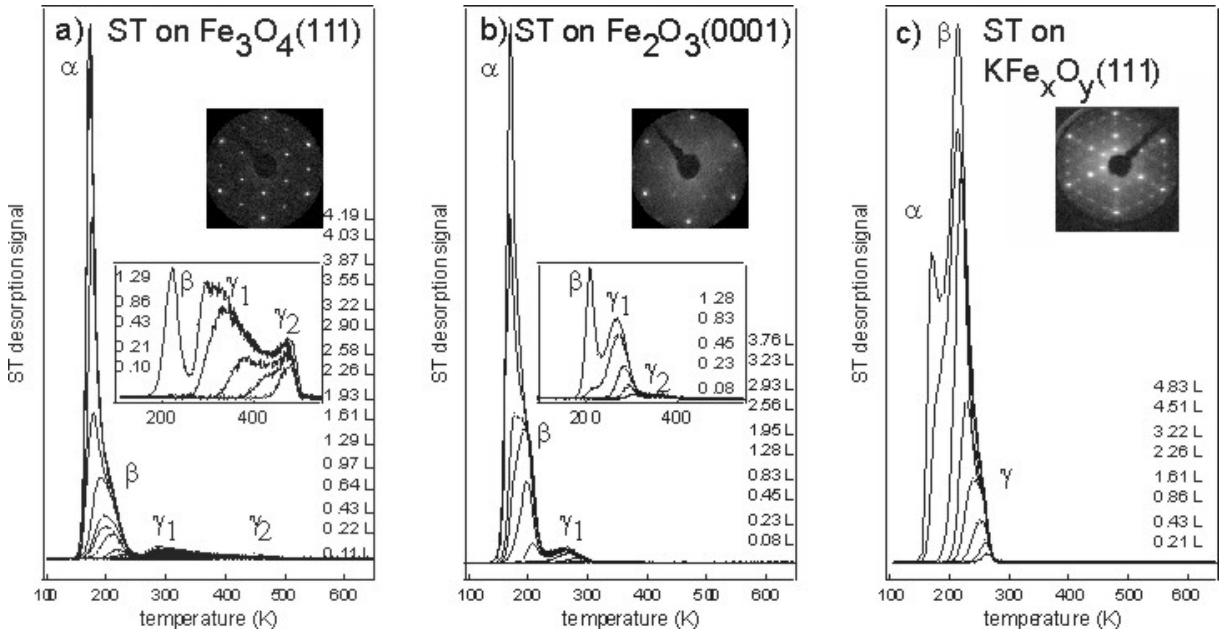

Fig. 2: TD spectra of styrene (St) absorbed at T=100 K onto Fe_3O_4(111), α-Fe_2O_3(0001) and KFe_xO_y(111). The exposures are given in Langmuir units. The inserts show magnified TD traces for low exposures.

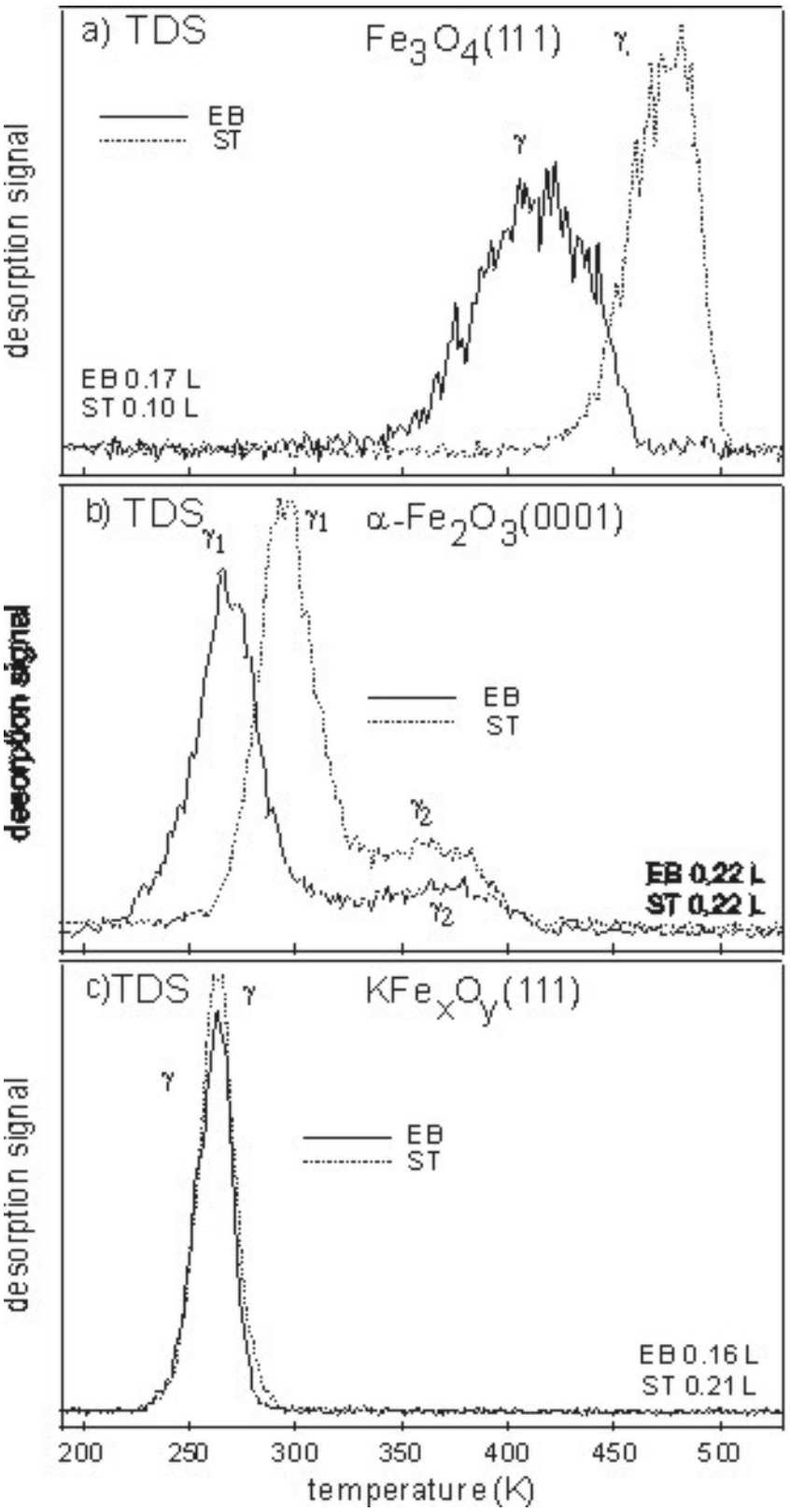

Fig. 3:
Comparison of TD traces of EB and St chemisorbed on $Fe_3O_4(111)$, α-$Fe_2O_3(0001)$ and $KFe_xO_y(111)$ taken upon low exposures.

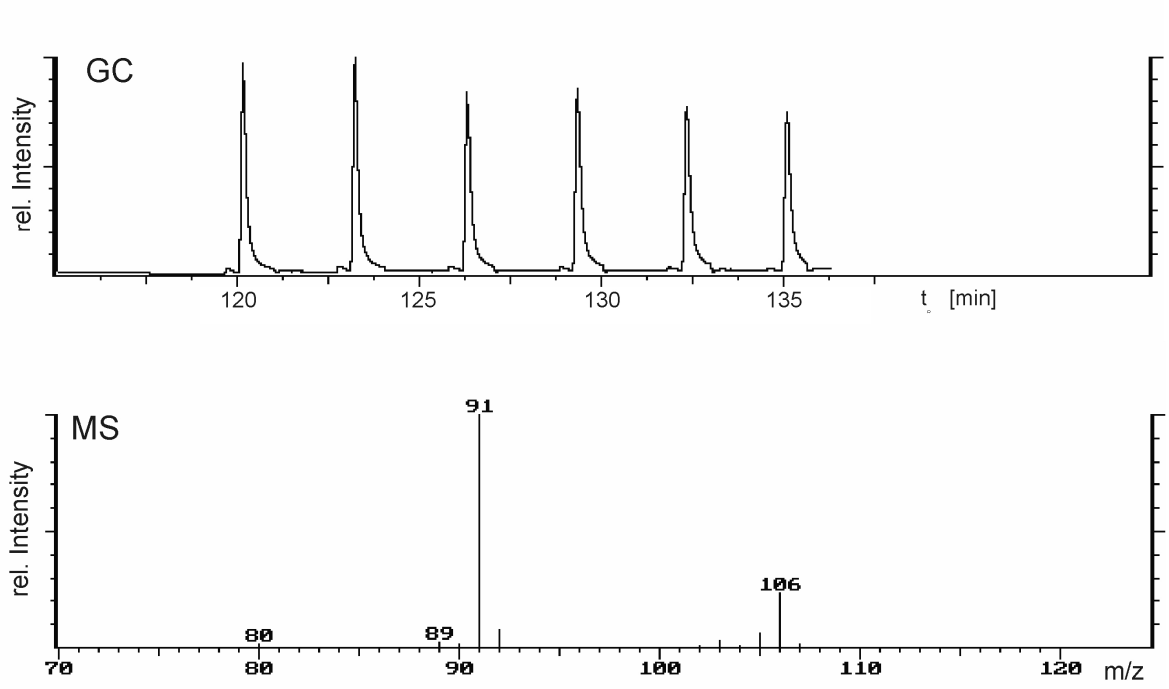

Fig. 4: Sequence of gas chromatograms over the reaction time t_R and mass spectrum from one GC peak for a reaction experiment performed on a $Fe_3O_4(111)$ film at 870 K. Gas leaving the reactor is injected into the column of the gas chromatograph every three minutes. Only the educt ethylbenzene (m/z=106 and its main cracking product m/z=91) is detected.

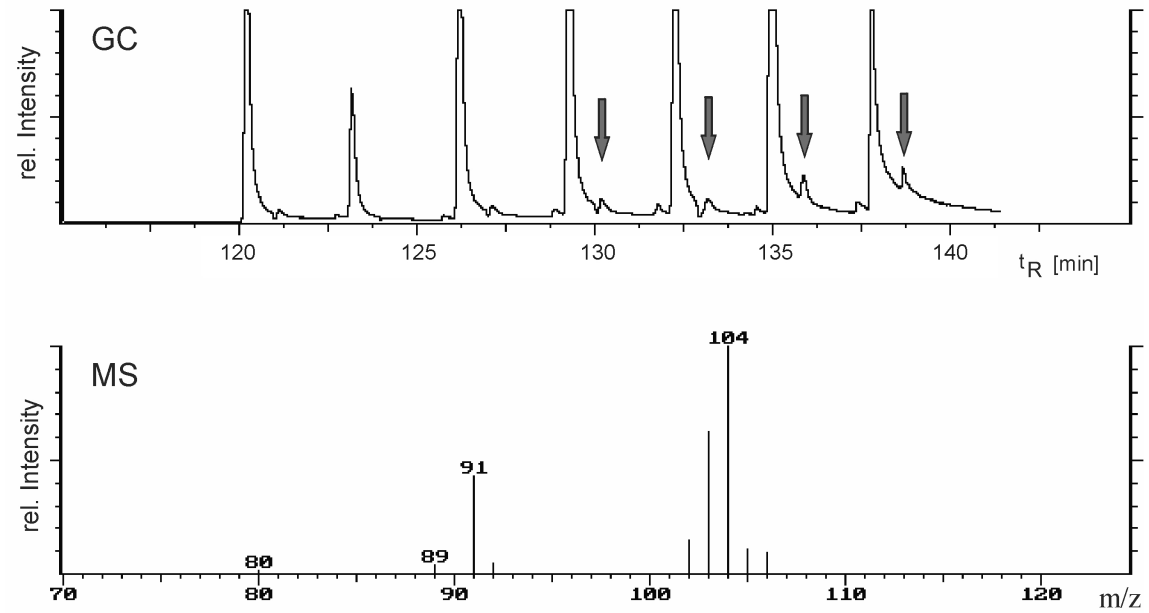

Fig. 5: Sequence of gas chromatograms and mass spectrum from a reaction experiment performed on a $KFe_xO_y(111)$ film at 870 K. Shown is the period of the reaction time t_R where a second peak marked by arrows develops. This small GC peaks represent styrene as shown by the mass spectrum below (m/z=104). Also EB (m/z=106, 91) is visible in the spectrum since the St-peak is superimposed on the tail of the big EB peak.

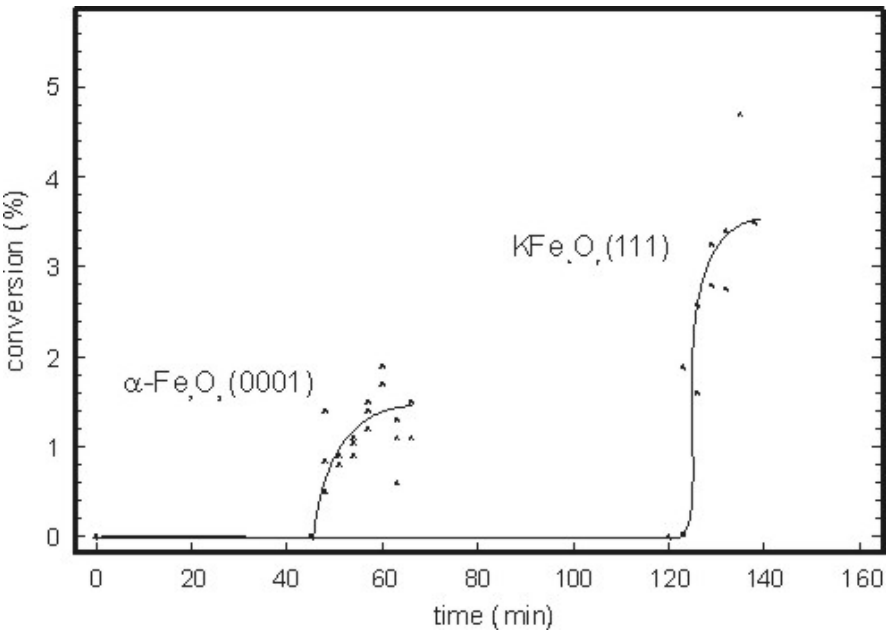

Fig. 6:
Conversion as function of time for the active films α-Fe_2O_3(0001) and KFe_xO_y(111). The conversion is given by the peak area ratio of styrene to ethylbenzene in the gas chromatograms like that in Fig. 5. After an activation period which is much longer for KFe_xO_y(111), the activity increases rapidly to the steady state.

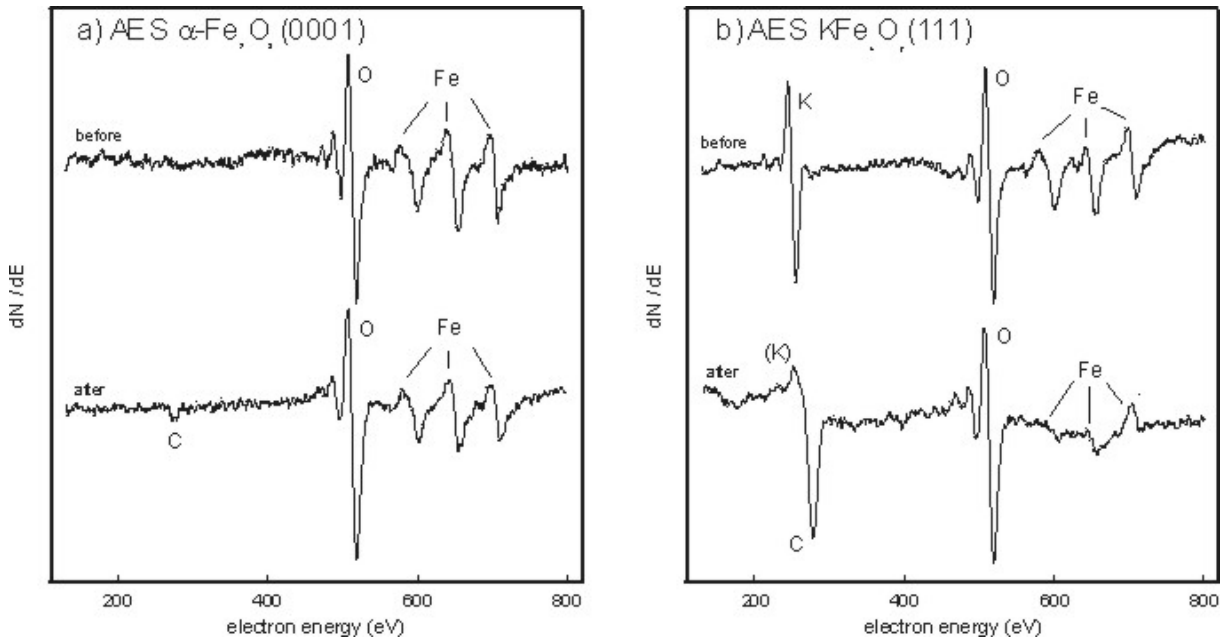

Fig. 7: Auger spectra of the α-Fe_2O_3(0001) and KFe_xO_y(111) films before and after the reaction experiment.

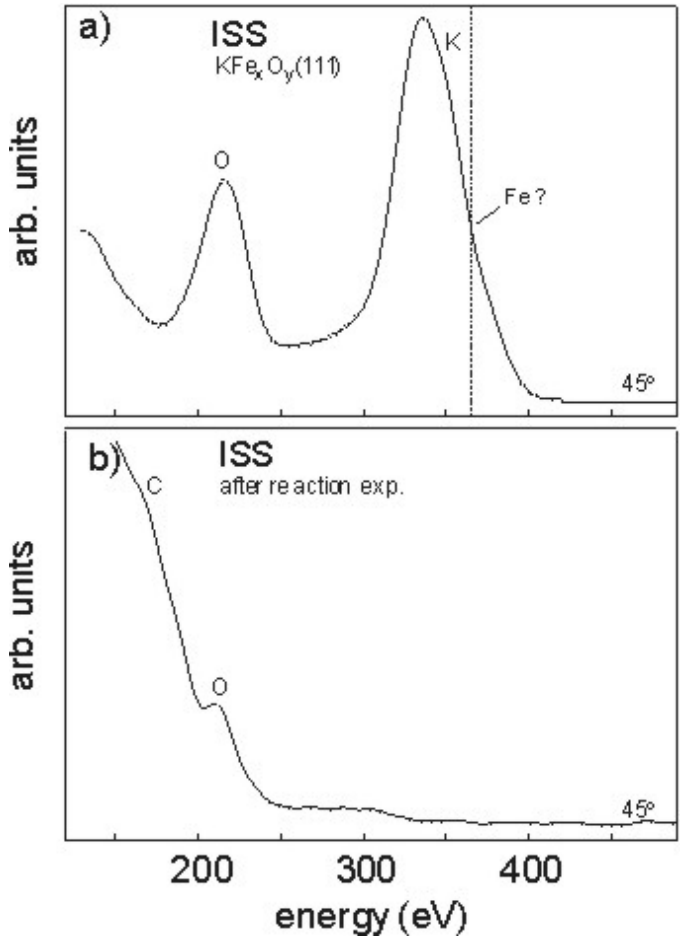

Fig. 8:
ISS spectra from the $KFe_xO_y(111)$ film before (a) and after the reaction experiment (b) recorded at an angle of 45° between incident ions and sample surface. The position where surface iron should appear is indicated.

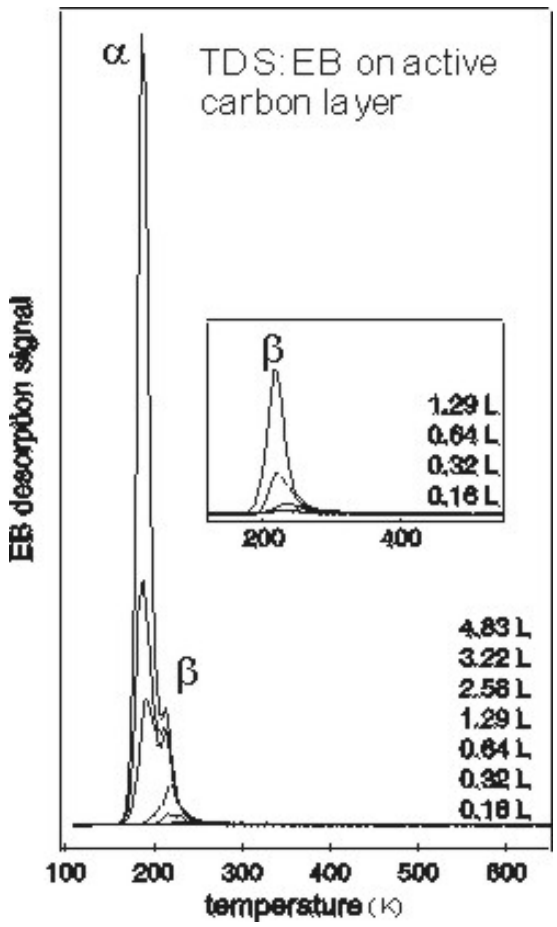

Fig. 9: TD spectra of ethylbenzene (EB) absorbed at T=100 K onto the carbon covered $KFe_xO_y(111)$ film, after the reaction experiment.

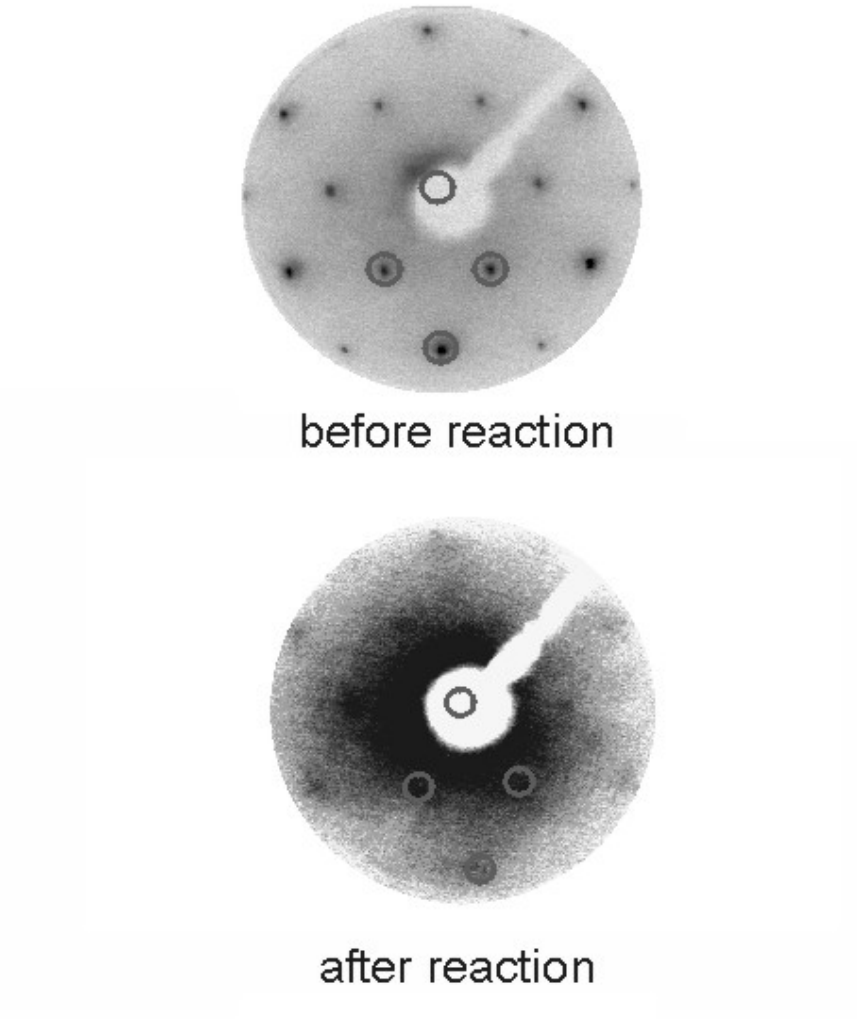

Fig. 10: LEED images of the α-Fe_2O_3(0001) film before and after a reaction experiment both taken at E=60 eV.

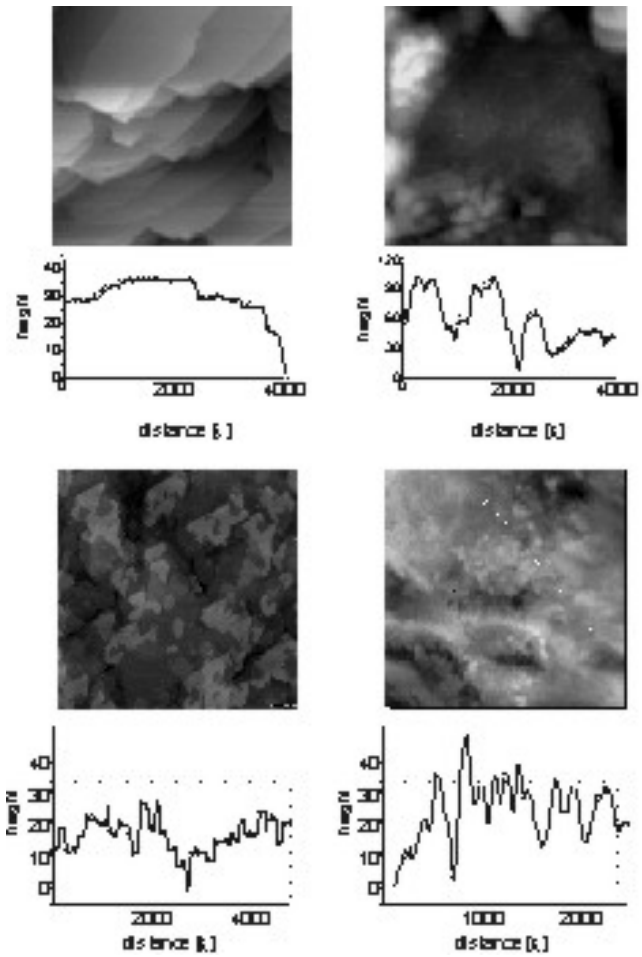

Fig. 11: Topographic STM survey images of the (a) α-Fe_2O_3(0001) and (b) KFe_xO_y(111) films before (left) and after (right) a reaction experiment. Height and length scales are given below the images.

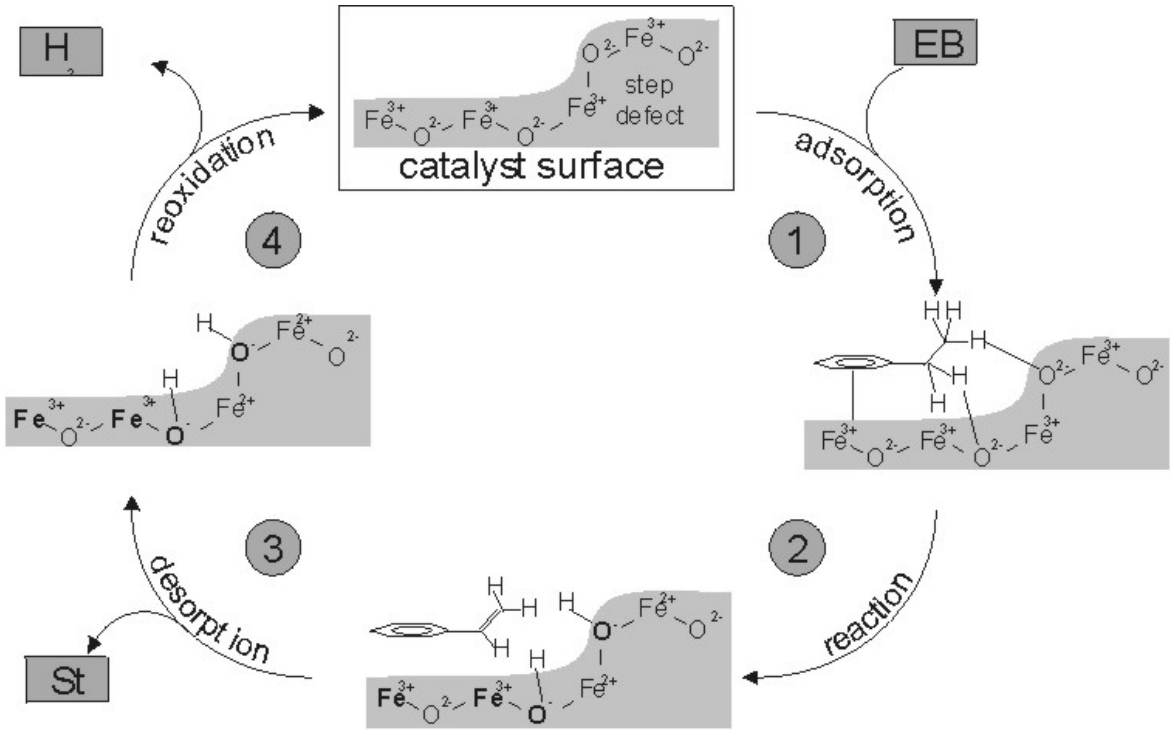

Fig. 12: Reaction scheme for the dehydrogenation of EB on defective α-Fe_2O_3(0001) model catalysts.